Desalination and Water Treatment
www.deswater.com

doi: 10.1080/19443994.2015.1126410

57 (2016) 23007–23018
October

Taylor & Francis
Taylor & Francis Group

Performance of a RED system with ammonium hydrogen carbonate solutions

M. Bevacqua[a], A. Carubia[a], A. Cipollina[a,*], A. Tamburini[a], M. Tedesco[b], G. Micale[a]

[a]*Dipartimento di Ingegneria Chimica Gestionale, Informatica, Meccanica (DICGIM), Università di Palermo (UNIPA) – viale delle Scienze Ed.6, 90128 Palermo, Italy, emails: maurizio.bevacqua@unipa.it (M. Bevacqua), antonio.carubia@gmail.com (A. Carubia), andrea.cipollina@unipa.it (A. Cipollina), alessandro.tamburini@unipa.it (A. Tamburini), giorgiod.maria.micale@unipa (G. Micale)*
[b]*Wetsus, European Centre of Excellence for Sustainable Water Technology, Oostergoweg 9, 8911 MA Leeuwarden, The Netherlands, email: Michele.Tedesco@wetsus.nl*

Received 15 April 2015; Accepted 22 November 2015

ABSTRACT

The use of closed-loop salinity gradient power (SGP) technologies has been recently presented as a viable option to generate power using low-grade heat, by coupling a SGP unit with a thermally-driven regeneration process in a closed loop where artificial solutions can be adopted for the conversion of heat into power. Among these, the closed-loop reverse electrodialysis (RED) process presents a number of advantages such as the direct production of electricity, the extreme flexibility in operating conditions and the recently demonstrated large potentials for industrial scale-up. Ammonium hydrogen carbonate (NH_4HCO_3) is a salt suitable for such closed-loop RED process thanks to its particular properties. At temperatures above 40–45°C, it decomposes into a gaseous phase containing NH_3, CO_2 and water. Thus, the use of NH_4HCO_3 solutions for feeding a RED unit would allow their easy regeneration (after the power generation step) just using low-temperature waste heat in a purposely designed regeneration unit. This work aims at presenting an experimental investigation performed on a RED system fed with NH_4HCO_3 solutions. Laboratory tests were carried out to find the best conditions for maximizing the power density and process performances of a RED unit by investigating a number of operating parameters such as fluid velocity and feed solutions concentration.

Keywords: Reverse electrodialysis; Salinity gradient power; Heat engine; Heat-to-power; Ammonium hydrogen carbonate

1. Introduction

Consumption of fossil fuels has dramatically increased in the last decades, reaching record levels year after year, with a global consumption often increasing more rapidly than production (e.g. 2.3% more in 2013) [1]. The spreading of renewable energy technologies is nowadays of paramount importance to meet the growing energy needs and reduce the use of fossil fuels. Within this context, energy from salinity

*Corresponding author.

Presented at EuroMed 2015: Desalination for Clean Water and Energy Palermo, Italy, 10–14 May 2015. Organized by the European Desalination Society.

gradients represents a promising source of sustainable energy [2,3].

A number of technologies have been proposed to harvest such energy for generating mechanical or electric energy. Among these, the most studied are pressure-retarded osmosis (PRO) and reverse electrodialysis (RED) [4,5]. In PRO, the salinity gradient is exploited to generate a water flux through a semi-permeable membrane, increasing the volume of the pressurised draw solution thus generating mechanical power by a hydraulic turbine [6,7]. Conversely, in RED process, the salinity gradient generates ion fluxes through ion exchange membranes; this ionic current is converted into electronic current on electrode surfaces, and finally collected by an external load [8–13].

Up to now, research activities for both PRO and RED have been mainly focused on the use of natural solutions as feed streams. In particular for the case of RED, different options have been investigated so far, from the use of river water and seawater (e.g. [14–16]) to the use of brackish water and concentrated brines [17,18].

The exploitation of natural salinity gradients is very promising, especially in coastal areas, where both dilute and concentrate streams can be available in large amount. On the other hand, using natural streams in SGP technologies have some remarkable drawbacks, such as geographical constraints for plant location and extensive pre-treatment costs to avoid fouling/biofouling phenomena in membrane modules.

Recently, a different application for SGP technologies has been proposed, where the SGP unit (either RED or PRO) operates in a closed loop using artificial saline solutions as working fluids. The exhausted solutions can be then regenerated through a proper regeneration step (either via an electrically-driven or a thermally driven process, acting as an energy storage or conversion technology, respectively), and sent back to the SGP stage [2]. Such "closed-loop SGP" system can be economically sustainable, for example, if a cheap source of thermal energy is available for the separation stage, e.g. waste heat from industrial processes. In this way, the system can be considered as a "SGP heat engine", where low-grade heat is converted into electricity by means of a SGP technology.

This concept was firstly proposed in the 1975 by Loeb [19] and then by Reali [20], who suggested the development of a closed loop PRO system where waste heat or energy from geothermal and volcanic sites could be exploited as thermal energy source for the regeneration step.

The use of artificial salinity gradients also allows exploring new possibilities in terms of unconventional salts and solvents [21], aiming at increasing the performance of the SGP heat engine, which is related to the ratio between the energy produced and the thermal energy required. In this regard, the use of thermolytic salts, such as ammonium hydrogen carbonate (NH_4HCO_3), has been recently presented as an interesting option for both RED [22–24] and PRO [25]. The peculiar property of NH_4HCO_3 is that it can be decomposed into ammonia, carbon dioxide and water by heating above 40–45˚C [26], thus allowing, in principle, to operate the regeneration step of the SGP heat engine at low temperature (i.e. using very low-grade heat).

Up to now, three different applications have been proposed in the literature for the exploitation of NH_4HCO_3 in SGP heat engines: the ammonia-carbon dioxide osmotic heat engine (OHE) [25], the thermal-driven electrochemical generator (TDEG) [22] and the concept of Microbial Reverse electrodialysis Cell (MRC) [24].

The ammonia-carbon dioxide OHE proposed by McGinnis et al. is a closed-loop PRO system where a NH_4HCO_3 solution is used as draw solution to create high osmotic pressures. A maximum thermal efficiency of 16% of the Carnot efficiency (likely corresponding to an actual energy conversion efficiency of 1.2%) has been predicted for an OHE that uses waste heat around 50˚C [25].

The TDEG presented in 2012 by Luo et al. [22] represents the first attempt to drive a RED process with NH_4HCO_3 solutions (as working fluids). Using a laboratory RED unit with 10 cell pairs, a maximum power density of $0.33\ W/m^2_{membrane}$ was obtained feeding the system with 0.02 M (dilute)–1.5 M (concentrate) NH_4HCO_3 solutions.

Another recent application of NH_4HCO_3 is represented by microbial RED systems in which a small RED stack is placed directly in contact with a microbial fuel cell (MFC), i.e. a biochemical reactor where exoelectrogenic bacteria are used to oxidize soluble organic matter, thus releasing electrons on an electrode surface. Using solutions with conductivity typical of domestic wastewater (~1 mS/cm), a power density over $3\ W/m^2$ of projected cathode area (i.e. over $0.3\ W/m^2$ of membrane area installed in the 5 cell-pairs set-up) has been reported in an MFC [24].

All these works suggest that employing ammonium bicarbonate solutions can be an interesting alternative to generate power by means of SGP-heat engines. Notwithstanding these promising features, insufficient data have been so far collected on the performance of a RED unit fed by NH_4HCO_3 solutions. The focus of the present work is on the experimental investigation of the performance of a lab-scale RED

unit operated with NH_4HCO_3 solutions. A number of different operating conditions including flow rates and salt concentrations were tested, thus providing more insight into the potential use of ammonium bicarbonate for RED closed-loop applications.

2. Experimental apparatus and procedures

2.1. Experimental apparatus

The experimental campaign was performed with a home-made RED module with $10 \times 10\ cm^2$ of membrane area. The repeating unit of the system (cell pair) is constituted by a cation exchange membrane (CEM), a dilute (LOW) compartment, an anion exchange membrane (AEM) and a concentrate (HIGH) compartment. The cell pair number was fixed at 10 for each test performed. During the operation, all the compartments are alternately fed with the two feed streams, thus generating a concentration gradient across all the membranes. The CEMs ideally allow only the transport of cations, rejecting anions; analogously, the AEMs allow the passage of anions, rejecting cations. Once the RED system is connected to a variable external electrical load, the resulting ionic currents are converted into electric current at the ends of the stack, where two electrodes are placed. A suitable redox couple (in this case, $K_3Fe(CN)_6/K_4Fe(CN)_6{\cdot}3H_2O$) is used in the electrode compartments for this purpose.

Ion exchange membranes provided by Fujifilm Manufacturing Europe BV (The Netherlands) and 270-μm woven spacers (Deukum GmbH, Germany) were used as stack components. The properties of the used IEMs are reported in Table 1.

Nafion® perfluorinated membranes (DuPont, USA) were employed in the electrode compartments, because of their very high selectivity towards the active redox species.

The electrode compartments contain Ru-Ir oxide-coated Ti electrodes (Magneto Special Anodes BV, The Netherlands). The electrode rinse solution (ERS) was composed of 0.1 M $K_3Fe(CN)_6$, 0.1 M $K_4Fe(CN)_6{\cdot}3H_2O$ (Chem-lab with purity 99.5%), adding 1 M NH_4HCO_3 as supporting electrolyte. A flow rate of 225 ml/min in the electrode compartments was kept for all the tests.

The test rig is constituted by the RED unit, plus four inlet/outlet tanks (20 l capacity) for both solutions and the required monitoring device, as sketched in Fig. 1.

Two peristaltic pumps (Cellai 530 U) were used to force the concentrate and the dilute solutions to flow within the RED unit. A similar peristaltic pump (Verderflex M025) was used for pumping the ERS from a glass tank covered by aluminium foil to avoid decomposition of the redox couple due to light exposure [27]. The relevant process variables (inlet-outlet pressure drops, stack voltage) were measured and collected via a data acquisition system (DAQ-National Instruments) and monitored through LabVIEW™ environment. The conductivity of the feed solutions (both at inlets and outlets) were measured by means of a conductivity meter (WTW LF196). A variable resistance (ranging between 0.7 and 54.8 Ω) was connected to the RED unit for testing the system under different load conditions. The feed solutions were prepared with demineralized water and ammonium hydrogen carbonate (Sigma–Aldrich, purity 99%).

2.2. Experimental procedures

2.2.1. Experimental measurement of power density

During the testing, the RED unit is connected to the calibrated external resistance (R_{ext}), and the stack voltage (E_{stack}) is recorded with a frequency of 1 Hz. Therefore, for each value of the external resistance (R_{ext}), the corresponding stack current is calculated by Ohm's law:

$$I_{stack} = \frac{E_{stack}}{R_{ext}} \quad (1)$$

Table 1
Properties of the two sets of IEMs adopted in the experiments*

Membrane	Thickness (μm)	Area resistance[a] (Ω cm^2)	Permselectivity[b] (%)	Ion exchange capacity (meq/g)
Fujifilm AEM RP1 80045-01	120	1.84	62	1.28
Fujifilm CEM RP1 80050-04	120	3.12	80	1.45

*Nominal data provided by membrane manufacturer using conventional (NaCl) solutions.
[a]Electrical resistance measured in 0.5 M NaCl solution at 25°C.
[b]Permselectivity measured in 0.05–5 M NaCl conditions at 25°C.

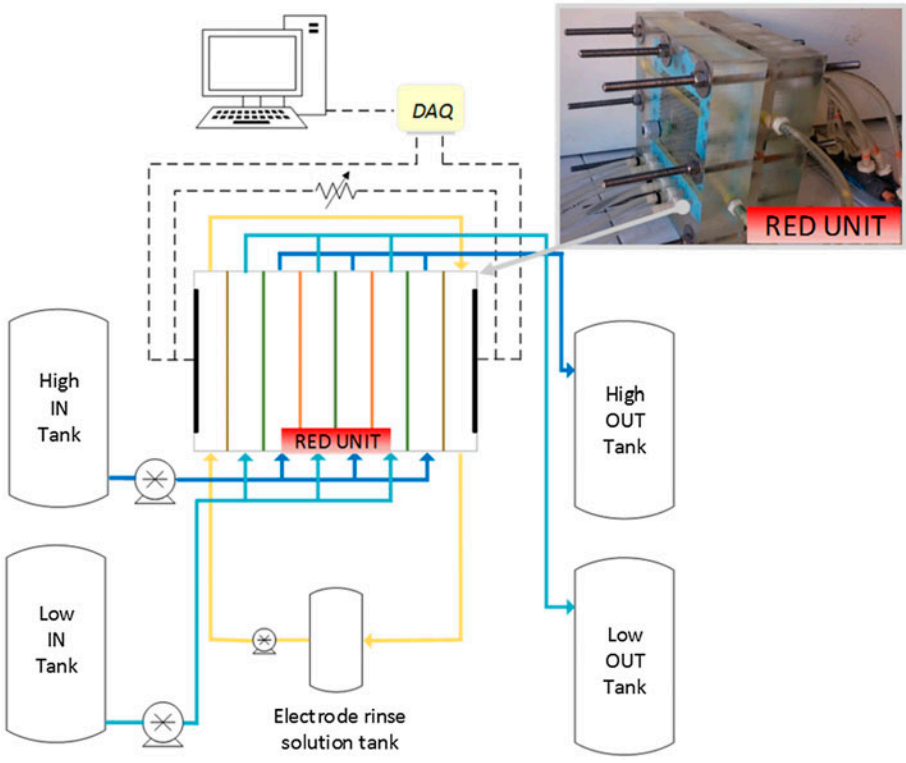

Fig. 1. Simplified scheme of the experimental apparatus. A picture of the RED unit used in the present work is reported in the upper-right corner of the figure.

The stack voltage is also equal to:

$$E_{stack} = OCV - R_{stack} \cdot I_{stack} \quad (2)$$

where OCV is the open circuit voltage (i.e. the stack voltage under zero-current conditions), and R_{stack} is the internal stack resistance (which can be assessed as the slope of the straight line in a E_{stack} vs. I_{stack} graph, see Fig. 3(A)). Thus, the electric power (P) is given by:

$$P = E_{stack} \cdot I_{stack} \quad (3)$$

The performance of a RED system is generally expressed as power density, i.e. the amount of power generated per cell pair area:

$$P_d = \frac{P}{N \cdot A} \quad (4)$$

where N is the number of cell pairs and A is the active area of one cell pair (Fig. 2(B)).

The net power density is calculated as the gross power minus the pumping power required (assuming 100% pumping efficiency):

$$P_{d,net} = \frac{P - \Delta p_{HIGH} \cdot Q^{tot}_{HIGH} - \Delta p_{LOW} \cdot Q^{tot}_{LOW}}{N \cdot A} \quad (5)$$

where Δp are the pressure drops and Q^{tot} is the total (i.e. sum of each channel flow rate) feed flow rate; subscripts HIGH and LOW refer to concentrate and dilute, respectively. Notably, for each operating condition tested, the concentrate and dilute solution were always fed with the same flow rate (i.e. $Q^{tot}_{HIGH} = Q^{tot}_{LOW}$). The corresponding pressure drops take into account the contribution relevant to the spacer-filled channel as well as that relevant to the inlet–outlet manifolds (e.g. distributor and collector) which in many cases may be the most prominent [28].

2.2.2. Evaluation of blank resistance and corrected power density

The power output values collected from laboratory-scale RED units are affected by the behaviour of the electrode compartments (generally identified with a so-called "blank-resistance", R_{blank}). Despite this, contribution is negligible on full-scale systems (i.e. where hundreds of cell pairs are piled in a single stack), it can be significant for a laboratory-scale unit.

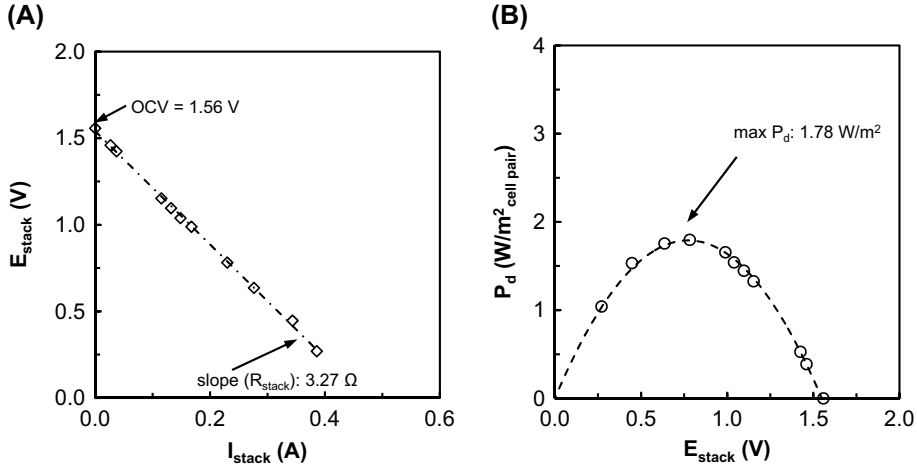

Fig. 2. Example of data measured/inferred by the experimental procedure: (A) E_{stack} vs. I_{stack}; (B) P_d vs. E_{stack}. RED stack (10 × 10 cm², 10 cell pairs) equipped with Fujifilm membranes, 270 μm woven spacers. C_{HIGH} = 2 M NH_4HCO_3; C_{LOW} = 0.02 M NH_4HCO_3; v = 1 cm/s, T = 293 K.

The blank resistance (R_{blank}) can be estimated as the stack resistance when the number of cell pairs approaches zero [29]. For this reason, the stack resistance was experimentally measured by varying the number of cell pairs (5, 10, 15, and 20), and a blank resistance of 1.07 Ω was obtained as intercept with y-axis on a R_{stack} vs. N plot.

Therefore, the internal resistance due to the cell pairs only (R_{cells}) can be calculated as:

$$R_{cells} = R_{stack} - R_{blank} \tag{6}$$

In this way, a corrected stack voltage can be estimated, disregarding the contribution of the blank resistance:

$$E_{stack,corr} = OCV - R_{cells} \cdot I_{corr} \tag{7}$$

where I_{corr} is the corrected current, calculated as:

$$I_{corr} = \frac{E_{stack,corr}}{R_{ext}} \tag{8}$$

Substituting Eq. (8) into Eq. (7) and rearranging, the corrected stack voltage is given by:

$$E_{stack,corr} = OCV - E_{stack,corr}\frac{R_{cells}}{R_{ext}} \tag{9}$$

Rearranging Eqs. (3), (4), (8), and (9), the corrected power density ($P_{d,corr}$) can be calculated as:

$$P_{d,corr} = \frac{OCV^2}{N \cdot A \cdot R_{ext}\left(1 + \frac{R_{cells}}{R_{ext}}\right)^2} \tag{10}$$

Eq. (10) provides the power density obtainable by a full-scale RED system operating under the same conditions of a laboratory-scale unit. Hence, it provides a reliable indication of the potential of the RED unit on a large scale (Fig. 3). Fig. 3 also shows the comparison between the relevant magnitudes of the corrected and uncorrected quantities previously described.

3. Results and discussion

The RED unit was tested under different operating conditions, changing the feed concentration of the dilute and the flow velocity of both solutions. For the concentrate solution, an inlet concentration of 2 M NH_4HCO_3 was adopted as standard for all tests: this allows to keep a high salinity ratio (i.e. ratio between C_{HIGH}/C_{LOW}), notwithstanding the relatively low solubility of ammonium bicarbonate in water (2.7 M at 298 K [30]). A summary of the tests presented in this work is reported in Table 2.

3.1. Influence of dilute concentration

The concentration of the dilute solution is a crucial factor for the performance of a RED system, since it affects both the driving force and the resistance of the stack. In particular, a careful selection of the feed dilute concentration can significantly enhance the

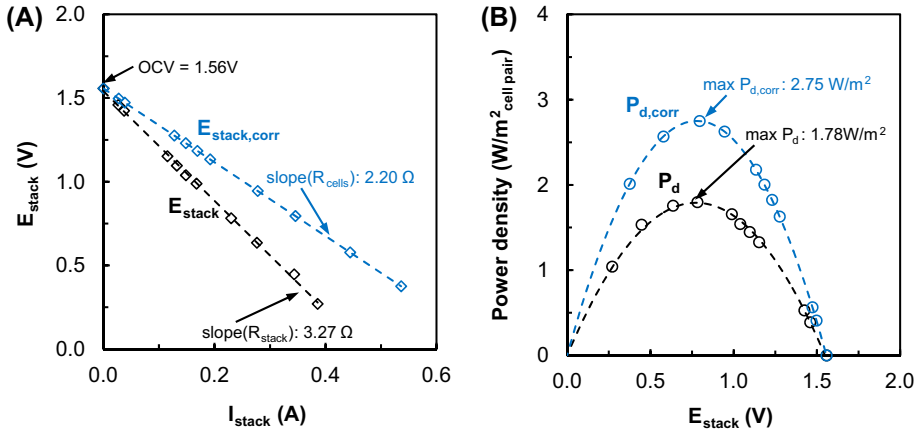

Fig. 3. Example of data measured/inferred by the experimental procedure: (A) E_{stack} vs I_{stack}; (B) Power density vs E_{stack}. Black dashed line case includes the blank resistance; blue dashed line case does not include the blank resistance. RED stack (10 x 10 cm^2, 10 cell pairs) equipped with Fujifilm membranes, 270 μm woven spacers. C_{HIGH} = 2 M NH_4HCO_3; C_{LOW} = 0.02 M NH_4HCO_3; v = 1 cm/s, T = 293 K.

Table 2
Summary of experimental tests presented in this work[a]

Relevant section	Main focus of the tests	Dilute concentration, C_{LOW} (M NH_4HCO_3)	Feed flow velocity, v (cm/s)
3.1	Influence of dilute concentration (C_{LOW})	0.01–0.02–0.04–0.06–0.1	1
3.2	Influence of feed flow velocity (v)	0.02–0.04	0.5–1–1.5–2

[a]Overall conditions: RED stack (10 × 10 cm^2, 10 cell pairs) equipped with Fujifilm membranes, 270-μm woven spacers. C_{HIGH} = 2 M NH_4HCO_3; T = 293 K.

power output. Notably, the electric resistance of the dilute can represent even the 50% of the whole stack resistance when fresh water (0.017 M NaCl) and seawater (0.5 M NaCl) are used as feed solutions [31].

In the case of RED process with NaCl solutions, the optimal dilute concentration to maximize the power output has been identified in the range of 0.01–0.1 M NaCl, depending on the stack design (e.g. channel thickness, membrane resistance) and operating conditions [32–34]. However, the use of unconventional salts such as ammonium bicarbonate requires a new investigation of the optimal concentration range maximizing the performance of the RED process. Moreover, when artificial solutions are used in a closed loop, feed concentrations are not dictated by those of natural sources, and can be purposely chosen for the process.

In this regard, the RED system was tested by changing the feed concentration of the dilute in the range of 0.01–0.1 M NH_4HCO_3. Relevant results are reported in Fig. 4: in particular, OCV and stack resistance are shown in Fig. 4(A), while the corresponding maximum values of power densities are reported in Fig. 4(B).

In the investigated range, the lower the dilute concentration, the higher the OCV and the stack resistance are expected (Fig. 4(A)). As a matter of fact, the reduction of dilute concentration corresponds to a higher salinity ratio, thus resulting in an increase of the OCV. Similarly, lowering the feed concentration also causes an increase of the electric resistance in the dilute compartments, which is the main contribution to the stack resistance. These phenomena have a counteracting effect on the power output, leading to a maximum in the gross power density (P_d = 1.78 $W/m^2_{cell\ pair}$) at C_{LOW} = 0.02 M (Fig. 4(B)).

OCV values and trend very similar to those presented here were found by Luo et al. [22]. Conversely, higher R_{stack} were reported by the same authors [22] allegedly due to the higher spacer thickness and to the different membranes employed (in their case: Selemion CMV and AMV, Asashi glass, Japan). Such a difference

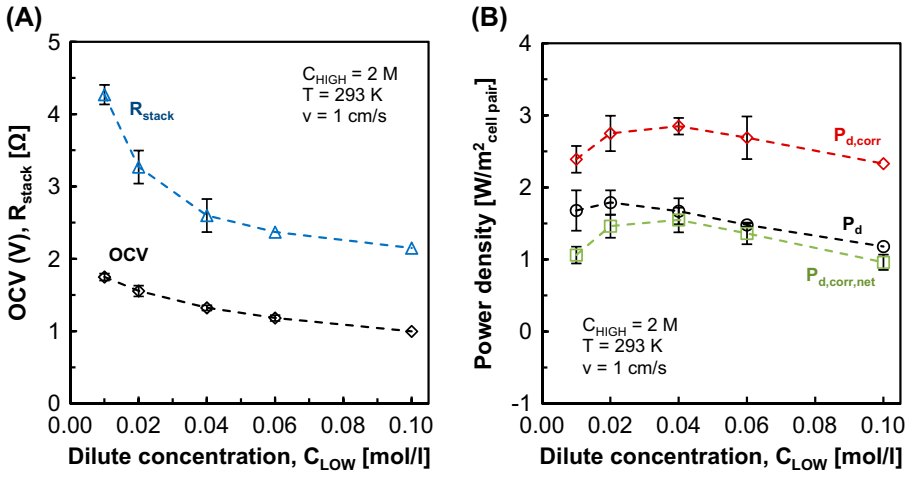

Fig. 4. Influence of dilute concentration on process performance. (A) OCV and stack resistance and (B) Gross power density, corrected gross power density, corrected net power density. RED stack (10 × 10 cm^2, 10 cell pairs) equipped with Fujifilm membranes, 270 μm woven spacers. C_{HIGH} = 2 M NH_4HCO_3; v = 1 cm/s, T = 293 K.

results in a P_d three times lower on average: they found a maximum P_d at C_{LOW} = 0.02 as in the present case, but equal to 0.66 $W/m^2_{cell\ pair}$.

Looking at the corrected power density ($P_{d,corr}$), a different (with respect to P_d) optimal value of C_{LOW} was observed (~0.04 M NH_4HCO_3), corresponding to a maximum value for $P_{d,corr}$ of 2.85 $W/m^2_{cell\ pair}$ (Fig. 4(B)).

Pressure losses were also measured and the relevant results are reported in Fig. 5. This figure shows that the concentration has an effect on pressure drop as expected on the basis of the difference in solution viscosity. Clearly, when only the concentration of the dilute solution is changed (see Table 2) only a very slight variation in pressure drop occurs.

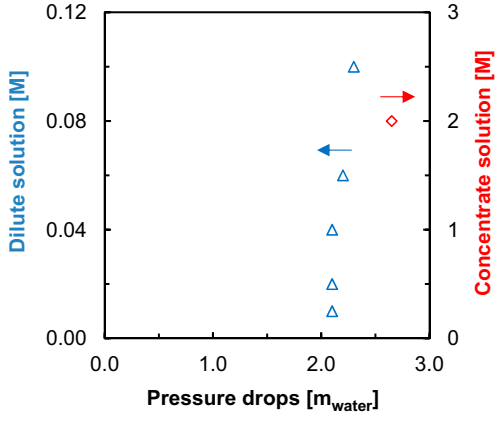

Fig. 5. Influence of dilute concentration on pressure drops. RED stack (10 x 10 cm^2, 10 cell pairs) equipped with Fujifilm membranes, 270 μm woven spacers. C_{HIGH} = 2 M NH_4HCO_3; v = 1 cm/s, T = 293 K.

By taking into account these hydraulic losses, the net corrected power density was estimated and reported in the same plot of $P_{d,corr}$ (Fig. 4(B)): a maximum value of 1.55 $W/m^2_{cell\ pair}$ was found at the same C_{LOW} of ~0.04 M as expected. For all tests, each value is provided with an error bar calculated using the maximum discrepancy among results relevant to some reproducibility tests. For the net power density, the experimental uncertainty was estimated by adopting the uncertainty definition given by Moffat [35,36].

Since the maximum power density was found at 0.02 M, while the maximum corrected power density was found at 0.04 M, the effect of dilute flow rate was investigated by fixing the dilute concentration at these two values (Table 2), as it will be presented in the next section.

3.2. Influence of feed flow velocity

In addition to the inlet concentration of feed solutions, another crucial parameter for the RED process is the flow velocity inside compartments, which also strongly affects the pressure drops, and hence the net power output.

The investigated RED system was tested assuming different flow velocities for both solutions, ranging from 0.5 up to 2 cm/s. Also, as mentioned above, two values of dilute concentration were tested (i.e. C_{LOW} equal to either 0.02 or 0.04): the results relevant to C_{LOW} = 0.02 M are reported in Fig. 6, while those at C_{LOW} = 0.04 M are shown in Fig. 8.

In Fig. 6(A) the effect of flow rate on OCV and relevant R_{stack} are reported. Notably, the former would be constant if membranes were ideal. In fact, its actual variation with flow rate is due to the non-perfect permselectivity of the membranes, which allow the passage of little amounts of salt and water. Results show that an increase of flow velocity provides a slight enhancement of the OCV in the first range (0.5–1 cm/s), until a plateau is reached (Fig. 6(A)). Such effect is mainly related to the lower residence time inside the stack that allows a practically constant driving force between inlet–outlet to be maintained. Higher flow rates also cause a reduction of polarization phenomena (especially in the dilute solution), which are, however, expected to be very low according to the very low fluxes occurring under open circuit conditions. Likewise, the flow rate has a double effect on R_{stack}: a low residence time corresponds to a small variation of the dilute channel conductivity thus leading to a high R_{stack}; on the other hand, a higher flow rate reduces concentration polarization phenomena (i.e. non-ohmic resistance) thereby providing lower R_{stack}. For the present case, the first effect appears to be prominent as an increase of R_{stack} with the flow rate was recorded (Fig. 6(A)). As a matter of fact, the resistance due to the dilute compartment, as shown in Fig. 6(A), represents around 30–40% of the stack resistance and its effect is determinant on the stack performance. Also Luo et al. [22] investigated the effect of feed flow rate on process performance. As already discussed for the case of Fig. 1, they reported OCV similar to those of the present work, while the stack resistance was much higher, thus resulting in three times lower P_d [22].

As a result of the simultaneous increase of competing variables as OCV and R_{stack}, the power density was found only slightly dependent on the flow rate: an average value of 1.81 and 2.81 $W/m^2_{cell\ pair}$ for P_d and $P_{d,corr}$ was found, respectively (Fig. 6(B)). As already discussed, the net corrected power density (Eq. (5)) can be calculated considering the pressure drops inside the dilute and concentrate compartments. As seen in Fig. 7(A), the experimental pressure drops increase as the feed flow velocity increases, but with a different slope depending on the solution concentration (i.e. different fluid-dynamic properties as density and viscosity). The two trends are linear, thus suggesting the existence of a stationary regime at the flow rate range investigated. The two trends were reported also in terms of non-dimensional numbers in Fig. 7(B): the void-channel Reynolds number (*Re*) and the void-channel fanning friction factor (*f*) defined as [10,37]:

$$Re = \frac{\rho \cdot v_{m,void} \cdot d_{h,void}}{\mu} = \frac{2 \cdot \rho \cdot v_{m,void} \cdot H}{\mu} \quad (11)$$

$$f = \frac{\Delta p}{l} \frac{d_{h,void}}{2 \cdot \rho \cdot v^2_{m,void}} \quad (12)$$

where v_m is the average velocity along the main flow direction in a corresponding spacer-less (void) channel, $d_{h,void}$ is twice the channel thickness H (270 μm in our case) and μ is the fluid viscosity (0.9 cP for the

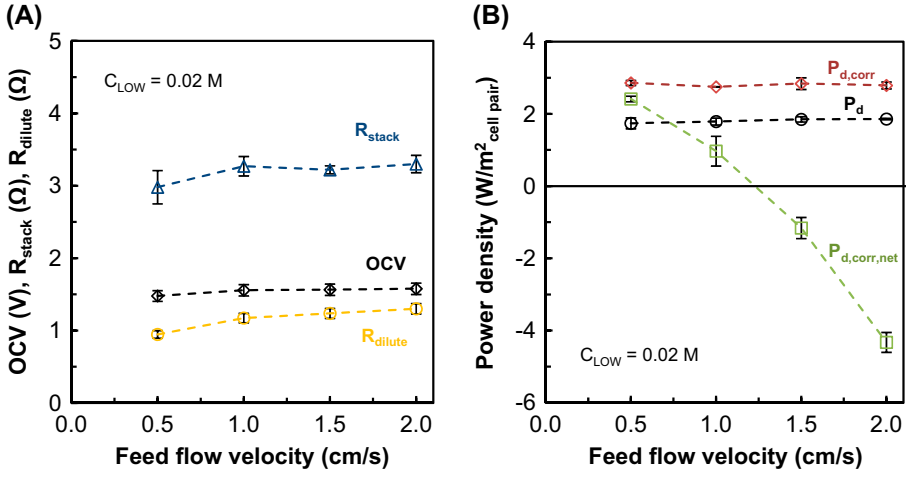

Fig. 6. Influence of feed flow velocity on process performance. (A) OCV, stack resistance, resistance of the dilute compartment. (B) Gross power density, corrected gross power density, corrected net power density. RED stack (10 × 10 cm^2, 10 cell pairs) equipped with Fujifilm membranes, 270 μm woven spacers. C_{HIGH} = 2 M; C_{LOW} = 0.02 M; T = 293 K.

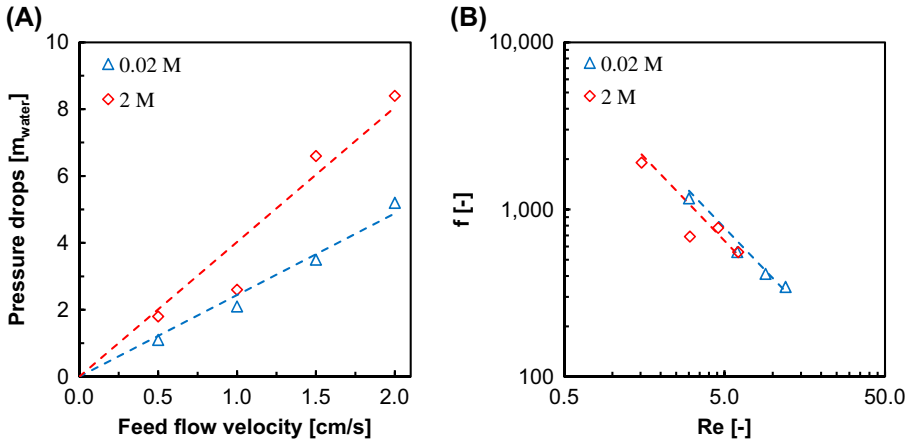

Fig. 7. Influence of feed flow velocity on the experimental pressure drops. (A) Experimental pressure drops values and (B) Fanning friction factor as a function of Reynolds number. RED stack (10 × 10 cm^2, 10 cell pairs) equipped with Fujifilm membranes, 270-μm woven spacers. C_{HIGH} = 2 M; C_{LOW} = 0.02 M; T = 293 K.

dilute solution and 1.88 cP for the concentrate). As it can be seen, the two trends are very similar to each other, being indeed almost overlapped. As a consequence, the $P_{d,corr,net}$ values were calculated using the linear trend instead of the experimental points.

The resulting $P_{d,corr,net}$ reported in Fig. 6(B) were found to be lower than zero for all flow velocities being higher than 1.25 cm/s (see Fig. 6(B)). As it can be seen, the lowest flow velocity (~0.5 cm/s) among those tested, was found preferable to maximize the net power density under the investigated conditions (Fig. 6(B)). Actually, even lower flow rates should be investigated in the future in order to recognize the maximum value of $P_{d,corr,net}$.

A similar test was performed for the case of a dilute concentration of 0.04 M NH_4HCO_3, which was the value maximizing the corrected power density (Fig. 4(B)). Corresponding results are shown in Fig. 8. Trends quite similar to those relevant to C_{LOW} = 0.02 M were found, with the main difference concerning the R_{stack} trend. As a difference from the case at C_{LOW} = 0.02 M, R_{stack} exhibits here a decreasing trend as the flow rate increases. This is allegedly due to the influence of polarization phenomena, which are in this case more relevant than the resident time effect (Fig. 8(A)): at this higher concentration (than the previous case), the dilute channel resistance is poorly dependent on the residence time (Fig. 8(A)).

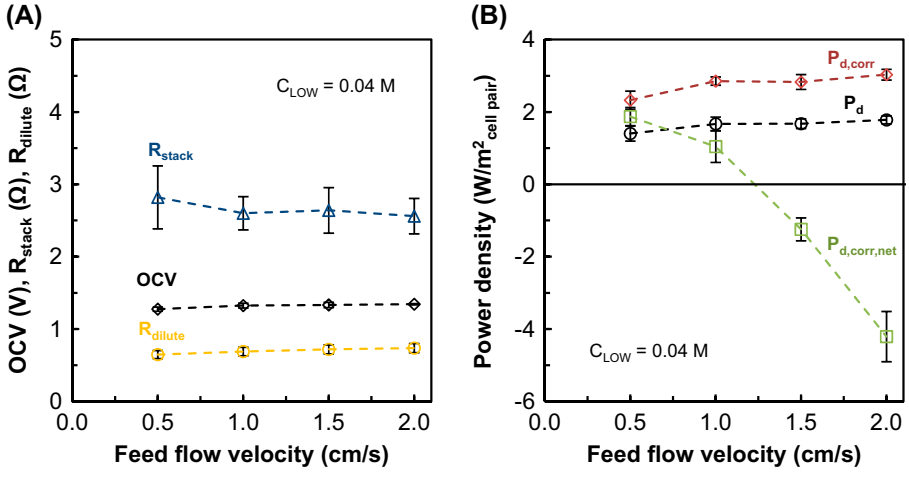

Fig. 8. Influence of feed flow velocity on process performance. (A) OCV, stack resistance, resistance of the dilute compartment and (B) Gross power density, corrected gross power density, corrected net power density. RED stack (10 × 10 cm^2, 10 cell pairs) equipped with Fujifilm membranes, 270-μm woven spacers. C_{HIGH} = 2 M; C_{LOW} = 0.04 M; T = 293 K.

The corrected net power density was calculated using the same procedure already described for the case of $C_{LOW} = 0.02$ M and is not reported again here.

These results confirm that (i) the highest power density is achieved at the lowest flow rate and that (ii) flow velocities higher than 1 cm/s are unsuitable for generating electric power from the RED unit adopted in the present study.

4. Conclusions

Recent works have proved that NH_4HCO_3-water solutions may be conveniently used in a RED-closed loop for converting low-grade waste heat into electric current. Aim of the present work was to investigate the performance of a lab-scale (i.e. 10×10 cm^2) RED unit fed by NH_4HCO_3-water solutions. In particular, the effect of dilute concentration and feed flow rate on gross power density were investigated. Pressure drops were also measured, thereby allowing the estimate of the net power density achievable. Results have shown that at a given flow rate (i.e. 1 cm/s) a dilute concentration of about 0.02–0.04 M guarantees the largest power output. At these values of concentration, under the conditions here investigated, a maximum net power output of 2.42 W/m$^2_{\text{cell pair}}$ can be obtained at the lowest feed flow velocity (i.e. 0.5 cm/s). On the other hand, feed flow rates higher than 1 cm/s lead to negative power output being the power loss due to pressure drop larger than the power production.

Overall, the use of ammonium bicarbonate allowed to reach values of power density comparable with the state-of-the-art of the RED process with conventional (NaCl) solutions [33], although membranes are not optimized yet for the use of this salt. Such finding suggests that ammonium bicarbonate could be a promising salt for the RED process. Furthermore, results highlight that the power density achieved in this work is three times higher than that reported by Luo et al. in a similar work [22] where the same salt is used. The main difference has been identified in the much lower stack resistance, likely due to an improved formulation of IEMs with a lower thickness and higher ionic conductivity, thus also emphasizing the potential for further technological improvements. Future work will deal with the "regeneration" of the NH_4HCO_3 solutions exiting from the RED-unit in order to assess the final feasibility of the RED heat engine for waste heat-to-power conversion.

Acknowledgements

This work has been performed within the RED-Heat-to-Power project (Conversion of Low Grade Heat to Power through closed loop Reverse Electro-Dialysis)—Horizon 2020 programme, Project Number: 640667: www.red-heat-to-power.eu. The authors are grateful to Fujifilm Manufacturing Europe BV for providing the membranes used during the experimental campaign. Thanks also to our workshop's master chief, Mr Giuseppe Fanale, for the support in building the experimental set-up.

Nomenclature

A	—	active area of one cell pair (m^2)
C	—	molar concentration (mol/l)
$d_{h,void}$	—	hydraulic diameter (m)
E_{stack}	—	stack voltage (V)
f	—	void fanning friction factor (–)
H	—	channel thickness (m)
I_{stack}	—	stack current (A)
l	—	channel length (m)
N	—	cell pairs number (–)
Δp	—	pressure drops (Pa)
P	—	electric power (W)
P_d	—	electric power density (W/m$^2_{\text{cell pair}}$)
Q^{tot}	—	total (i.e. inclusive of all channels) feed flow rate (m^3/s)
R_{blank}	—	blank resistance (Ω)
R_{cells}	—	cell pairs resistance (Ω)
R_{dilute}	—	resistance of dilute solution (Ω)
Re	—	void Reynolds number (–)
R_{ext}	—	external resistance (Ω)
R_{stack}	—	internal stack resistance (Ω)
T	—	temperature (K)
v	—	velocity (cm/s)
$v_{m,void}$	—	mean velocity along the main flow direction (void channel) (cm/s)

Greek letters

ρ	—	solution density (kg m^{-3})
μ	—	solution dynamic viscosity (Pa s)

Subscripts

corr	—	corrected value (of power output, stack voltage, stack current) obtained by using the stack resistance without the contribute of the blank resistance
HIGH	—	concentrate solution
LOW	—	dilute solution
net	—	net value (of power output) measured after subtracting the power losses due to the pumping of feed solutions

Acronyms

AEM	—	anion exchange membrane
CEM	—	cation exchange membrane
DAQ	—	data acquisition system
ERS	—	electrode rise solution
IEM	—	ion exchange membrane
MFC	—	microbial fuel cell
OCV	—	open circuit voltage (V)
OHE	—	osmotic heat engine
PRO	—	pressure retarded osmosis
RED	—	reverse electrodialysis
SGP	—	salinity gradient power
TDEG	—	thermal driven electrochemical generator

References

[1] BP, BP Statistical Review of World Energy June, (2014).

[2] B.E. Logan, M. Elimelech, Membrane based processes for sustainable power generation using water, Nature 488 (2012) 313–319.

[3] G.Z. Ramon, B.J. Feinberg, E.M.V. Hoek, Membrane-based production of salinity-gradient power, Energy Environ. Sci. 4 (2011) 4423–4434.

[4] A. Cipollina, F. Giacalone, F. Grisafi, G. Micale, A. Tamburini, G. Vella, Lab-scale investigation of a pressure retarded osmosis module fed by salinity gradients, Desalin. Water Treat. (in press).

[5] N.Y. Yip, M. Elimelech, Comparison of energy efficiency and power density in pressure retarded osmosis and reverse electrodialysis, Environ. Sci. Technol. 48 (2014) 11002–11012.

[6] A. Achilli, A.E. Childress, Pressure retarded osmosis: From the vision of Sidney Loeb to the first prototype installation—Review, Desalination 261 (2010) 205–211.

[7] A. Yaroshchuk, Optimal hydrostatic counter-pressure in Pressure-Retarded Osmosis with composite/asymmetric membranes, J. Membr. Sci. 477 (2015) 157–160.

[8] A. Tamburini, G. La Barbera, A. Cipollina, M. Ciofalo, G. Micale, CFD simulation of channels for direct and reverse electrodialysis, Desalin. Water Treat. 48 (2012) 370–389.

[9] A. Tamburini, G. La Barbera, A. Cipollina, G. Micale, M. Ciofalo, CFD prediction of scalar transport in thin channels for reverse electrodialysis, Desalin. Water Treat. 55 (2014) 3424–3445.

[10] L. Gurreri, A. Tamburini, A. Cipollina, G. Micale, M. Ciofalo, CFD prediction of concentration polarization phenomena in spacer-filled channels for reverse electrodialysis, J. Membr. Sci. 468 (2014) 133–148.

[11] D.A. Vermaas, J. Veerman, N.Y. Yip, M. Elimelech, M. Saakes, K. Nijmeijer, High efficiency in energy generation from salinity gradients with reverse electrodialysis, ACS Sustainable Chem. Eng. 1 (2013) 1295–1302.

[12] D.A. Vermaas, J. Veerman, M. Saakes, K. Nijmeijer, Influence of multivalent ions on renewable energy generation in reverse electrodialysis, Energy Environ. Sci. 7 (2014) 1434–1445.

[13] M. Tedesco, C. Scalici, D. Vaccari, A. Cipollina, A. Tamburini, G. Micale, Performance of the first reverse electrodialysis pilot plant for power production from saline waters and concentrated brines, J. Membr. Sci. 500 (2016) 33–45, doi: 10.1016/j.memsci.2015.10.057.

[14] J. Veerman, M. Saakes, S.J. Metz, G.J. Harmsen, Electrical power from sea and river water by reverse electrodialysis: A first step from the laboratory to a real power plant, Environ. Sci. Technol. 44 (2010) 9207–9212.

[15] A. Daniilidis, D.A.A. Vermaas, R. Herber, K. Nijmeijer, Experimentally obtainable energy from mixing river water, seawater or brines with reverse electrodialysis, Renewable Energy 64 (2014) 123–131.

[16] D.A. Vermaas, J. Veerman, N.Y. Yip, M. Elimelech, M. Saakes, K. Nijmeijer, High efficiency in energy generation from salinity gradients with reverse electrodialysis, ACS Sustainable Chem. Eng. 1 (2013) 1295–1302.

[17] M. Tedesco, A. Cipollina, A. Tamburini, G. Micale, J. Helsen, M. Papapetrou, REAPower: Use of desalination brine for power production through reverse electrodialysis, Desalin. Water Treat. 53 (2015) 3161–3169.

[18] E. Brauns, Towards a worldwide sustainable and simultaneous large-scale production of renewable energy and potable water through salinity gradient power by combining reversed electrodialysis and solar power Desalination 219 (2008) 312–323.

[19] S. Loeb, Method and apparatus for generating power utilizing pressure retarded osmosis, US Patent 3,906,250, Ben-Gurion University of the Negev Research and Development Authority, Beersheva, Israel, US (1975).

[20] M. Reali, Closed cycle osmotic power plants for electric power production, Energy 5 (1980) 325–329.

[21] E. Shaulsky, C. Boo, S. Lin, M. Elimelech, Membrane-based osmotic heat engine with organic solvent for enhanced power generation from low-grade heat, Environ. Sci. Technol. 49 (2015) 5820–5827.

[22] X. Luo, X. Cao, Y. Mo, K. Xiao, X. Zhang, P. Liang, X. Huang, Power generation by coupling reverse electrodialysis and ammonium bicarbonate: Implication for recovery of waste heat, Electrochem. Commun. 19 (2012) 25–28.

[23] M.C. Hatzell, B. Logan, Evaluation of flow fields on bubble removal and system performance in an ammonium bicarbonate reverse electrodialysis stack, J. Membr. Sci. 446 (2013) 449–455.

[24] R.D. Cusick, Y. Kim, B.E. Logan, Energy capture from thermolytic solutions in microbial reverse-electrodialysis cells, Science 335 (2012) 1474–1477.

[25] R.L. McGinnis, J.R. McCutcheon, M. Elimelech, A novel ammonia-carbon dioxide osmotic heat engine for power generation, J. Membr. Sci. 305 (2007) 13–19.

[26] F. Ullman, Ullmann's Encyclopedia of Industrial Chemistry, Wiley-VCH Verlag GmbH, Weinheim, (2005) 1499.

[27] O. Scialdone, C. Guarisco, S. Grispo, A.D. Angelo, A. Galia, Investigation of electrode material—Redox couple systems for reverse electrodialysis processes. Part I: Iron redox couples, J. Electroanal. Chem. 681 (2012) 66–75.

[28] L. Gurreri, A. Tamburini, A. Cipollina, G. Micale, M. Ciofalo, Pressure drop in woven-spacer-filled channels for reverse electrodialysis: CFD prediction and experimental validation, Desalin. Water Treat. (in press).

[29] M. Tedesco, A. Cipollina, A. Tamburini, W. van Baak, G. Micale, Modelling the Reverse ElectroDialysis process with seawater and concentrated brines, Desalin. Water Treat. 49 (2012) 404–424.
[30] R.H. Perry, D.W. Green, J.O. Maloney, Perry's Chemical Engineers' Handbook, McGraw-Hill, New York, NY, 2008.
[31] J. Veerman, M. Saakes, S.J. Metz, G.J. Harmsen, Reverse electrodialysis: Performance of a stack with 50 cells on the mixing of sea and river water, J. Membr. Sci. 327 (2009) 136–144.
[32] M. Tedesco, A. Cipollina, A. Tamburini, I.D.L. Bogle, G. Micale, A simulation tool for analysis and design of reverse electrodialysis using concentrated brines, Chem. Eng. Res. Des. 93 (2015) 441–456.
[33] M. Tedesco, E. Brauns, A. Cipollina, G. Micale, P. Modica, G. Russo, J. Helsen, Reverse electrodialysis with saline waters and concentrated brines: A laboratory investigation towards technology scale-up, J. Membr. Sci. 492 (2015) 9–20.
[34] A. Daniilidis, D.A.A. Vermaas, R. Herber, K. Nijmeijer, Experimentally obtainable energy from mixing river water, seawater or brines with reverse electrodialysis, Renewable Energy 64 (2014) 123–131.
[35] R.J. Moffat, Describing the uncertainties in experimental results, Exp. Therm. Fluid Sci. 1 (1988) 3–17.
[36] A. Tamburini, P. Pitò, A. Cipollina, G. Micale, M. Ciofalo, A thermochromic liquid crystals image analysis technique to investigate temperature polarization in spacer-filled channels for membrane distillation, J. Membr. Sci. 447 (2013) 260–273.
[37] L. Gurreri, A. Tamburini, A. Cipollina, G. Micale, M. Ciofalo, Flow and mass transfer in spacer-filled channels for reverse electrodialysis: A CFD parametrical study, J. Membr. Sci. 497 (2016) 300–317.